Quantitative Algorithm for Airborne Gamma Spectrum of Large Sample Based on Improved Shuffled Frog Leaping-Particle Swarm Optimization Convolutional Neural Network

Fei LI[1,2], Xiaofei HUANG[1], Yuelu CHEN[1], Binghai LI[3,4], Tang WANG[1], Feng CHENG[1,2,*], Guoqiang ZENG[1,2,*] & Muhao ZHANG[1,2]

[1] College of Nuclear Technology and Automation Engineering, Chengdu University of Technology, Chengdu 610000, China

[2] Applied Nuclear Technology in Geosciences Key Laboratory of Sichuan Province, Chengdu 610000, China

[3] Airborne Survey and Remote Sensing Center of Nuclear Industry, Shijiazhuang 050000, China

[4] Hebei Key Laboratory of Airborne Detection and Remote Sensing Technology, Shijiazhuang 050000, China

Fei Li: proposed research questions
Fei Li: designed experiments
Fei Li, Xiao-fei Huang, Bing-hai Li, Feng Cheng, Guo-qiang Zeng, Mu-hao Zhang: proposed algorithms
Fei Li, Xiao-fei Huang, Bing-hai Li, Feng Cheng, Guo-qiang Zeng, Mu-hao Zhang: verified raw data and analyzed
Fei Li, Xiao-fei Huang, Yue-lu Chen, Tang Wang: wrote the first draft
Fei Li, Xiao-fei Huang, Yue-lu Chen: revised the paper

This work was supported by the National Natural Science Foundation of China (No. 42127807), Natural Science Foundation of Sichuan Province (Nos. 23NSFSCC0116 and 2022NSFSC12333), and the Nuclear Energy Development Project (No. [2021]-88).
* Corresponding author: Feng Cheng (E-mail: chengfeng@cdut.cn), Guoqiang Zeng (E-mail: zgq@cdut.edu.cn).

Abstract

Objective: In airborne gamma ray spectrum processing, different analysis methods, technical requirements, analysis models, and calculation methods need to be established. To meet the engineering practice requirements of airborne gamma-ray measurements and improve computational efficiency, an improved shuffled frog leaping algorithm–particle swarm optimization convolutional neural network (SFLA-PSO CNN) for large-sample quantitative analysis of airborne gamma-ray spectra is proposed herein.

Methods: This method was used to train the weight of the neural network, optimize the structure of the network, delete redundant connections, and enable the neural network to acquire the capability of quantitative spectrum processing. In full-spectrum data processing, this method can perform the functions of energy spectrum peak searching and peak area calculations. After network training, the mean SNR and RMSE of the spectral lines were 31.27 and 2.75, respectively, satisfying the demand for noise reduction. To test the processing ability of the algorithm in large samples of airborne gamma spectra, this study considered the measured data from the Saihangaobi survey area as an example to conduct data spectral analysis.

Results: The results show that calculation of the single-peak area takes only 0.13~0.15 ms, and the average relative errors of the peak area in the U, Th, and K spectra are 3.11%, 9.50%, and 6.18%, indicating the high processing efficiency and accuracy of this algorithm.

Limitations: The performance of the model can be further improved by optimizing related parameters, but it can already meet the requirements of practical engineering measurement.

Conclusions: This study provides a new idea for the full-spectrum processing of airborne gamma rays.

Keywords: Large sample; Airborne gamma spectrum (AGS); Shuffled frog leaping algorithm (SFLA); Particle swarm optimization (PSO); Convolutional neural network (CNN)

1. Introduction

The International Atomic Energy Agency's "standard three-window method," also known as the "window data processing method," is the fundamental component of the conventional airborne gamma-ray spectrum data processing technique [1-2]. This approach is frequently used in data processing software, including Oasis Montaj [3] and AGRS GeoProbe [4], which provide a standard three-window data-processing module. In 1992, Wang Ping developed the "clustering analysis-based normalization method" based on the statistical analysis method to process the airborne gamma-ray spectrum data of three mining areas, providing more comprehensive information [5]. This was achieved to fully utilize the multiparameter data of the airborne gamma-ray spectrum and study the local radioactive anomaly region. Issues with peak position drift, energy scale, and radioactive statistical fluctuations that affected the accuracy of the analysis were resolved in 1993 by Yufeng et al. [6]. They also established mathematical and physical models for gamma-spectrum analysis and discussed the viability of the spectral method in software systems. In 2001, Hendriks combined an efficient BGO scintillator detector with full energy spectral data analysis (FSA) using the complete energy spectrum combined with the standard spectrum to calculate the ^{40}K, ^{232}Th, ^{238}U radioactivity concentrations [7]. In 2003, Guo Yufeng proposed a smoothing filtering method to solve the problem of statistical fluctuations in the natural gamma spectrum [8], compared the smoothing filtering effect of the natural gamma spectrum of two groups of core samples, and found that the error of the filtered spectrum was smaller than that of the unprocessed spectrum through theoretical derivation.

In the early 21st century, with the application of airborne gamma-ray spectrometry in the search for deep-blind deposits and in-situ sandstone type uranium deposits, users put forward higher requirements for the accuracy and efficiency of airborne gamma-ray spectrometry. Advances in electronics have facilitated the implementation of complex algorithms. In 2011, Weichong established a source-term analysis and measurement model for airborne gamma-spectrum measurements [9]. The airborne gamma spectrum is a composite of various source-term spectral components. In addition, the respective method directly solves the atmospheric radon correction problem without requiring additional up-detection detectors. In 2018, Ya et al. established a stratigraphic response model to compensate for the spectrum of the current depth with data from adjacent depth points, and achieved consistency between the energy scale of the measuring instrument with that of the standard instrument through spectral smoothing and drift correction [10]. In 2021, Gu Yi et al. derived the theory of minimum detectable activity concentration (MDAC) of the airborne gamma ray spectrum, and studied the relationship between the MDAC and the scintillation counter's intrinsic efficiency, scintillation crystal volume and energy resolution, and aircraft flight altitude [11].

Thus far, most data processing for airborne gamma-ray spectra has focused on the statistical fluctuation of a single spectrum. However, with the application of airborne gamma spectrometry in radioactive background investigations [12], nuclear accident emergency airborne gamma spectrometry [13-15], groundwater investigation [16], terrain correction and anomaly information recognition, among other fields [17-19], the processing technology of large-sample airborne gamma spectrometry data has developed over the past 10 years, from the optimization of spectral solution steps to the upgrading of spectral data system processing. In 2013, Shao Jiewen et al. developed gamma spectrum processing software according to the measurement requirements by integrating functions such as format conversion, batch spectrum solving, spectrum merging, and spectrum deduction of spectral files [20]. In 2017, George Lasche developed an application, Visual RobFit (VRF), for analyzing high-resolution gamma ray spectra using nonlinear fitting techniques to fit the full spectrum [21]. Automatic analysis of ^{228}Ra and ^{226}Ra from 12 soil samples and a consistent comparison with the analysis using a well-known commercial software demonstrated that this method better identifies overlapping peaks. In 2022, Feng Chunyuan et al. completely implemented the airborne gamma-ray full spectrum analysis method based on Python and its rich third-party class library programming, and solved the problem that large matrices can only be calculated using other numerical computing software; but its drawbacks are also obvious: the programming is complicated, the data processing efficiency is not high, and the relative error of the three-window method is up to 6.1% [22]. However, in an actual aerial gamma-spectrum detection mission, a single flight mission in a single measuring

area often returns a very large amount of line data, including at least tens of thousands of spectral lines [23]. Neural networks can learn and extract different patterns from large amounts of data, thus saving time and computational resources. To free researchers from tedious accelerator tuning tasks, Zhou Liuyuan developed a noninvasive diagnostic method based on convolutional neural network (CNN) and the interior point method with knowledge of scattering parameters [24]. However, there are currently no reports on large-sample, fast processing, high-precision algorithms, or software for airborne gamma measurement missions [25-26].

Based on the above problems, this study focused on the data characteristics of large samples. The particle swarm optimization (PSO) neural network was employed as the main algorithm [27], and combined with an improved shuffled frog-leaping algorithm based on simulated annealing to establish a new optimization network model. SFLA-PSO does not require calculation of the gradient, and considers both global and local optimizations. This algorithm is adopted to optimize the weight and bias of the CNN, which reduces the risk of the CNN algorithm falling into a local area, improves the training efficiency of the neural network, and accelerates the convergence rate of the network. In this study, the calibration data of the spectrum of the standard gamma field were used as the training set for model training. The trained model was verified during an airborne gamma-measurement mission in the Saihangaobi mining area.

2. Algorithm and model

2.1 Improved shuffled forg leapfrog algorithm

The shuffled frog leaping algorithm (SFLA), a new heuristic population intelligent evolution algorithm, simulates the population coevolution process of a group of frogs when searching for most food locations. It combines deterministic and random methods, and has high computational power and global search performance. To solve the problem in which the SFLA easily falls into a local optimum and the accuracy decreases, this study improves the SFLA based on a simulated annealing model. The Metropolis discriminant criterion in the simulated annealing algorithm is then used to improve the optimization ability of the SFLA.

2.1.1 Simulated annealing model

Ordinary simulated annealing algorithms produce only one new solution at a time, and based on the Metropolis criterion, the probability is determined to choose whether to accept the new state or not. Assuming the solution of the current moment search is x_t, the corresponding system energy (objective function) is E_t, and random disturbance is applied to the search point to generate a new solution x_{t+1}. Correspondingly, if the system energy is E_{t+1}, then the acceptance probability of the transition from x_t to x_{t+1} of the search point is:

$$P=\begin{cases} 1, & E_{t+1}<E_t \\ e^{\frac{-(E_{t+1}-E_t)}{kT}}, & E_{t+1}>E_t \end{cases} \tag{1}$$

2.1.2 Threshold oscillation SFLA model based on simulated annealing

To solve the problem of the SFLA easily falling into the local optima and its accuracy decreasing, this study improves the SFLA based on the simulated annealing model. The improved algorithm added a threshold shock strategy based on a simulated annealing strategy [28-29]. In the optimization process of the SFLA, all the populations participating in the population iteration accelerate to converge. The current frog population convergence was determined by the standard deviation of the frog solution in the community. When the mean deviation of each frog population decreases by a preset threshold, part of the population is divided into groups that oscillate near the optimal solution in their community, thus jumping out of the local optimum [30-32].

$$\begin{cases} U(t)=[M^{m/2+k} \mid (k=-\frac{m*\omega}{2},-\frac{m*\omega}{2}+1,...,\frac{m*\omega}{2}),\ k\neq 0, m*\omega\%2=0)] \\ U(t)=[M^{m/2+k} \mid (k=\frac{-m*\omega+1}{2},\frac{-m*\omega+1}{2}+1,...,\frac{m*\omega-1}{2}), m*\omega\%2=1)] \end{cases} \quad (2)$$

where, M represents frog memeplex, N frogs are allocated to $m/2+k$ populations and each memeplex contains n frogs, satisfying $N=m\times n$, ω is the proportion of the number of groups that are mapped out to the total number of groups. When the spatial standard deviation of the S-dimension solution of the frog memeplex meets the threshold value, several memeplex are selected successively from the middle segment memeplex to both sides of each memeplex, and the sampled memeplex is defined as the regional oscillating memeplex. $U(t)$ indicates rearrangement of M in descending order for the evolution iteration of the next generation memeplex [33]. The specific algorithm flow is shown in Fig. 1.

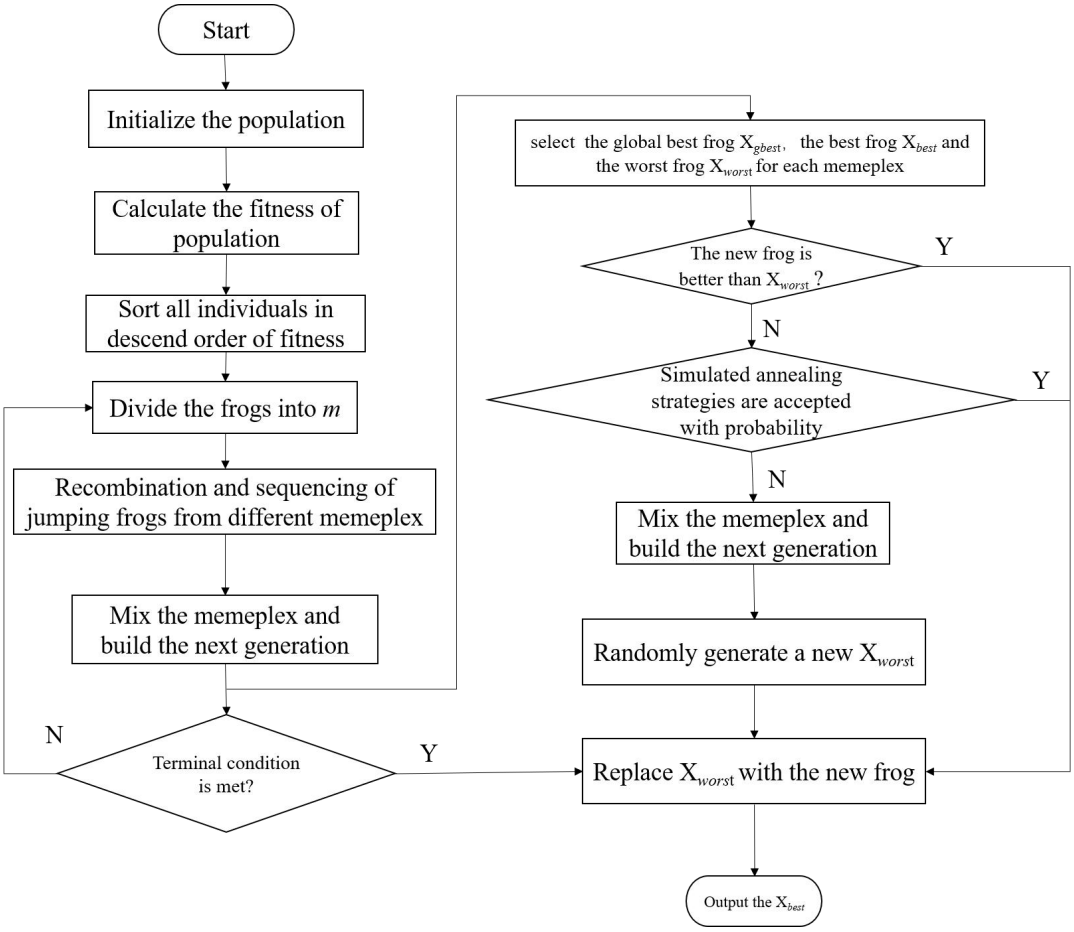

Fig. 1 Improved SFLA global search process

2.2 PSO neural network model

The evolutionary computing method known as PSO was developed based on an investigation of flock predation behavior. The fundamental objective of PSO is to determine the most effective solution through group collaboration and knowledge exchange. The organizational structure of a social network significantly affects the PSO performance. The degree of connectedness between network nodes, the number of clusters, and the separation between nodes affect how information moves between networks. Fig. 2(b) depicts a typical PSO global optimum social network structure. Communication occurs between the particles, and the social network structure of the globally optimal

PSO is a star topology. In this structure, part of the particle velocity update reflects the information obtained from all particles in the population.

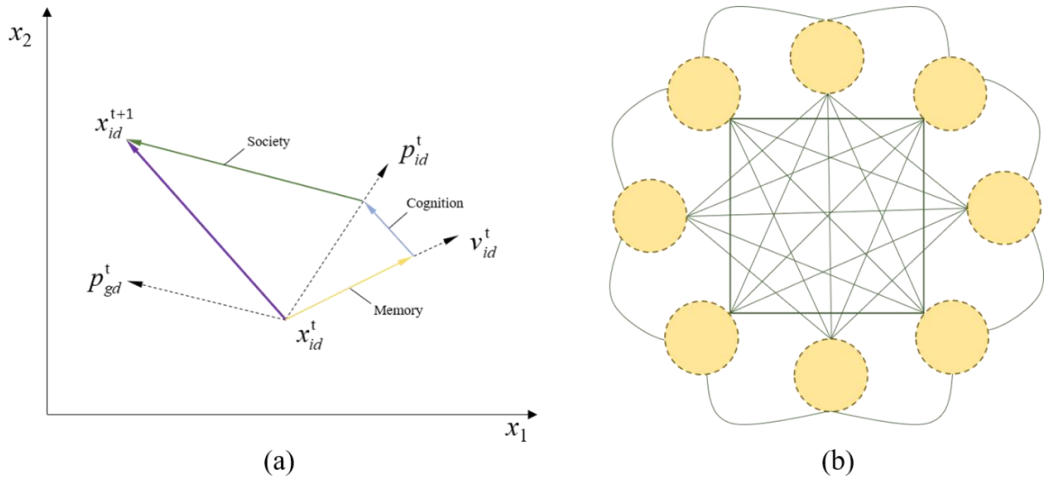

Fig. 2 (a) Particle migration mode in solution space (b) Global optimal PSO network structure

In Fig. 2 (a), x_{id}^{t} represents the starting position of the particle, x_{id}^{t+1} is the position of the particle at the next moment; v_{id}^{t} is for the speed at which particles "fly"; p_{id}^{t} represents the current optimal position of the searched particle, p_{gd}^{t} represents the global optimal location. In a globally optimal PSO network, the particle velocity is

$$v_{ij}(t+1)=v_{ij}(t)+c_1\cdot r_{1j}(t)\cdot[y_{ij}(t)-x_{ij}(t)]+c_2\cdot r_{2j}(t)\cdot[y_{ij}(t)-x_{ij}(t)] \tag{3}$$

$v_{ij}(t)$ is the velocity of particle i in the j dimension, $x_{ij}(t)$ is the position of particle i in the j dimension. $y_{ij}(t)$ is the best position of particle i in the j dimension, $j=1,2,...,n_x$. c_1,c_2 is the acceleration constant (used to measure the contribution degree of cognitive part, social part), $r_{1j}(t),r_{2j}(t)\sim U(0,1)$ are the random values sampled from the uniform distribution.

Because of its advantages of being straightforward and simple to apply without requiring numerous parameter adjustments, PSO has been widely employed in function optimization, neural network training, fuzzy system control, and other genetic algorithm applications. For example, in digital alpha spectrum peak seek, Mohamed S. El_Tokhy coupled antlion optimizer and PSO to peak finder algorithm, solved the second-order pileup caused by high count rate, and obtained a faster and more accurate peak finder method [34]. To explore the optimization effect of PSO, this study sets the matrix definition domain space to 200×200, and sets x∈[-200,200] and y∈[-200,200] , taking the Gaussian function as the objective function of PSO.

$$f(x)=\frac{1}{2\pi\sigma^2}e^{-\frac{x^2+y^2}{2\sigma^2}} \tag{4}$$

The PSO network model is constructed by Matlab. To obtain the maximum value of the Gaussian function within the range of the matrix, all the values in the matrix can be directly traversed, and the maximum value can then be obtained. PSO is used to constantly update the velocity and position of particles in the grid space, move them in the direction of the optimal solution, and quickly shorten the time required to obtain the optimal solution, which can significantly improve computational efficiency. In the search for the maximum value problem, the update of $y_i(t)$ satisfies:

$$y_i(t+1)=\begin{cases} y_i(t), f(x_i(t+1))\le f(y_i(t)) \\ y_i(t+1), f(x_i(t+1))> f(y_i(t)) \end{cases} \tag{5}$$

where, $f:R^{n_x}\rightarrow R$ is the fitness function.

In a globally optimal particle swarm network, a particle can communicate with many other particles, and this interaction promotes information exchange among particles; subsequently, the population converges to the optimal solution. Fig. 3 shows the operation results of the PSO searching

for the maximum value of the Gaussian function. The green dots in (a) represent optimal particle positions. In (b), "Loss" represents the error of the model during each iteration, "Epoch" represents the number of iterations of data in the training process. It can be seen that the algorithm converges to the approximate optimal value after more than 20 iterations.

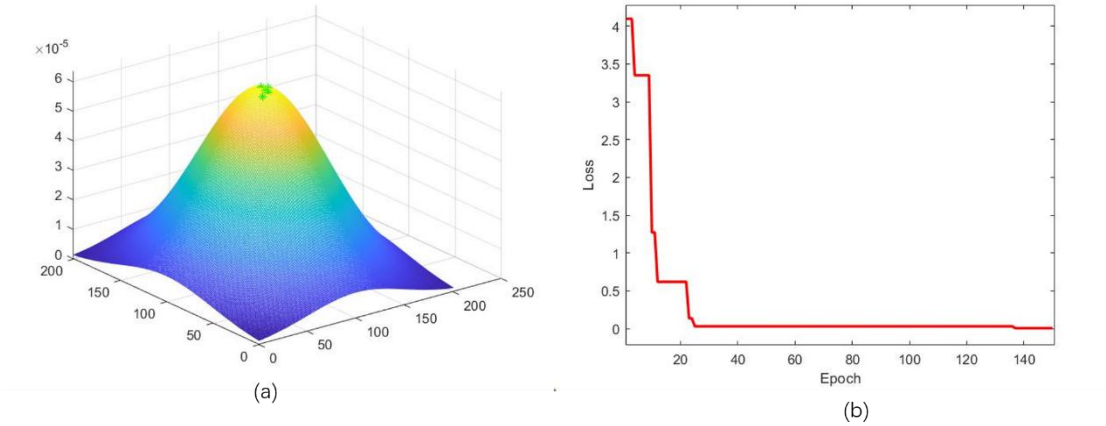

Fig. 3 Optimization results of particle swarm optimization algorithm

The basic idea of the SFLA-PSO CNN is to replace the random gradient descent with an optimization algorithm, update the weight and structure of the network, and realize the process of back propagation. Using a global search optimization algorithm, an initial weight matrix and bias vector can be obtained to obtain the final neural network structure.

3. Results and Discussion

3.1 Data sources

In this study, measured airborne gamma-ray full-spectrum data of aerial remote areas in Hebei province and the Saihangaobi deposit in the Inner Mongolia region were selected, including the survey line, base point, measuring date, time, active time, temperature, radar height, barometric height, K, U, Th, energy spectrum window width and 0-255 channels of down-spectrum data. The training data comprised the energy spectrum data of the Beijing Aerial Remote Sensing Standard Gamma Field. The file size was 82.1 MB and the file format was ".dat," containing tens of thousands of spectral data. This type of large-sample processing is extremely demanding for gamma spectrum processing systems. Saihangaobi testing zone data were used as practical test data to verify the effects of the trained model.

3.2 Standard gamma spectrum model training

3.2.1 Setting Model Parameters

First, the initial parameters were set. The input layer set the input size to 256 px. The 256 channels of the full-spectrum data contained U, Th, and K nuclide information. Setting the Epoch to 32 and iteration time to 150. The population size of the PSO algorithm used to optimize the neural net is $n=40$. The initial inertia weight $w=0.9$, which linearly reduces to 0.4 as the number of iterations gradually diminishes the influence of the prior particle velocity on the present velocity, and the acceleration constant $c_1=c_2=2$ [35-37]. Each population contained 100 frogs, the number of iterations within each population was 10, the number of global information exchanges was 50, and the attenuation coefficient D of the simulated annealing strategy was a random number between 0.3 and 0.5. The populations were divided into ten groups based on a thresholding oscillation mixed leapfrog algorithm using simulated annealing. The oscillating intervals were 0.01, 0.05, 0.1, and 0.2, of the value range of the independent variables [38].

Common CNN use convolutional and pooling layers instead of fully connected layers. Through deep learning, that is, an increase in the number of layers, the model learns more abstract features. This study adopted the CNN structure shown in Fig. 4 and set two convolution pooling layers: a fully connected layer and an output layer. Spectral data were entered from the left side of a 16 × 16 grid. After the feature extraction of the convolutional and pooling layers, the coefficients of the fully connected layers were updated using the improved SFLA-PSO. After network training, a new spectral line on the right side was obtained as the output.

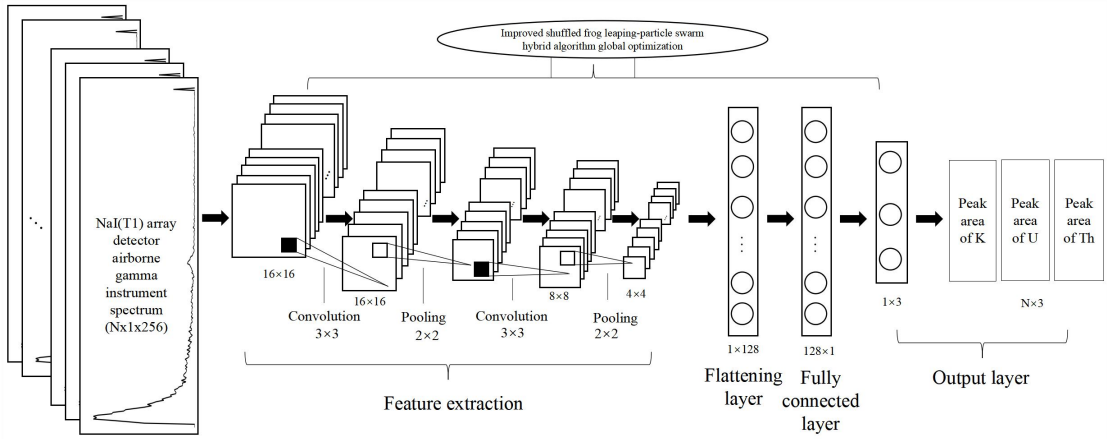

Fig. 4 SFLA-PSO CNN model structure

3.2.2 Spectrum processing and analysis

The gamma spectrum data measured by the NaI (TI) detector were processed and analyzed using 256 experimental data points [39-40]. The improved SFLA-PSO neural network algorithm was used to process the measured spectrum [41], and the processing and results of the measured data were analyzed from two aspects: spectrum line comparison and signal-to-noise ratio before and after processing to verify the rationality of the model design in this study and test the noise reduction effect [42].

To objectively analyze the model effect, the special energy spectrum data, maximum peak area (Fig. 5), minimum peak area (Fig. 6), and spectrum of the average peak area (Fig. 7) were simultaneously analyzed.

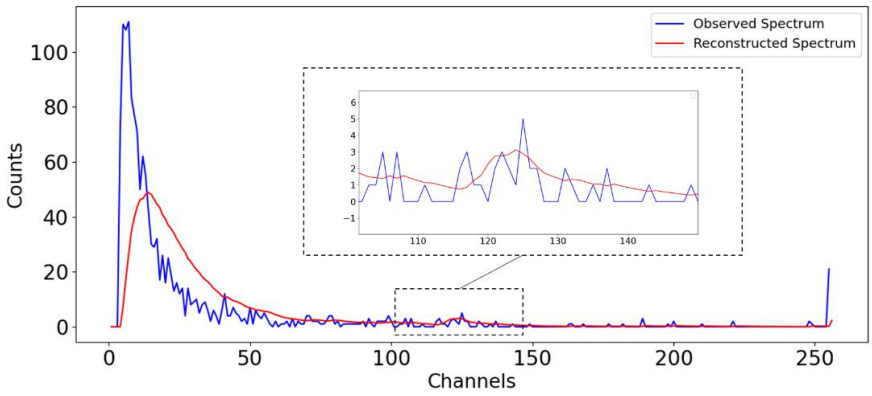

Fig. 5 Graph of maximum peak area spectra

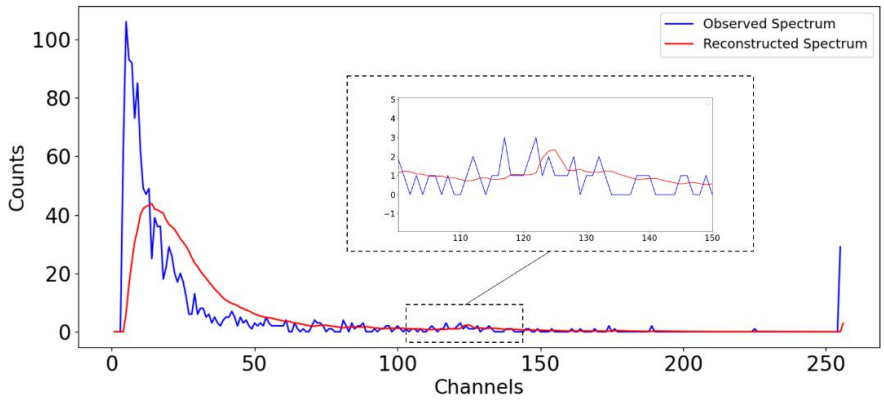

Fig. 6 Comparison diagram of minimum peak area spectral line

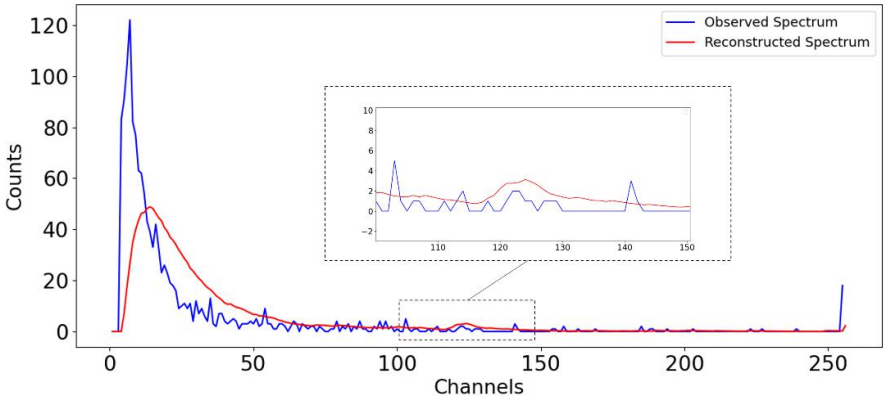

Fig. 7 Comparison of spectral lines of average peak area

By comparing the spectra of the airborne gamma ray spectrometer before and after calibration and recombination, it can be seen that after model training and recombination, the noise information in the spectrum was significantly reduced, and the information of the weak peaks was preserved. For the weak peak region in the maximum peak area spectrum (Fig. 5), the reconstructed spectrum not only removes noise information but also preserves and highlights the weak peak shape. In the minimum peak area spectrum (Fig. 6) before reconstruction, the weak peak information was hidden in the noise. After reconstruction, weak peak information was enhanced. In the average peak area spectrum (Fig. 7), the reconstructed spectrum also had significant effects on noise reduction and highlighted weak peaks.

To assess the ability of this model to extract spectral data, the signal-to-noise ratio was quantitatively analyzed after energy spectrum training. Equation (6) was used to calculate the signal-to-noise ratio (SNR), where $y(n)$ represents the predicted value, $\tilde{y}(n)$ represents the true value, and N_b represents the sample size.

The higher the expected value, the better the noise-reduction ability of this model.

$$\mathrm{SNR} = 10\log_{10}\frac{\sum_{n=1}^{N_b} y^2(n)}{\sum_{n=1}^{N_b}(y(n)-y(n))^2} \tag{6}$$

The RMSE is the square root of the ratio of the deviation between the predicted and real values and the observed number, which is used to measure the deviation between the denoised and original

spectra. According to Equation (7), the smaller the value, the higher the SNR and the more effective the training model in reducing noise.

$$\mathrm{RMSE}=\sqrt{\sum_{n=1}^{N_b}\frac{(y(n)-y(n))^2}{N_b}} \tag{7}$$

In this study, 160 groups of reconstructed spectral data were selected to calculate the signal-to-noise ratio; the results are shown in Fig. 8.

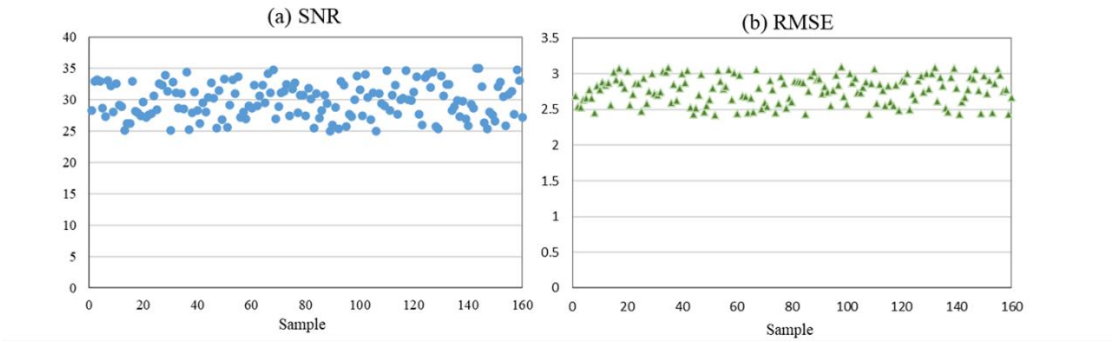

Fig. 8 (a) Reconstituted spectrum SNR (b) reconstituted spectrum RMSE

Referring to the experimental results of Li Fei [43], the SNR value is generally approximately 30 and the RMSE value should be less than 10. After wavelet denoising was performed on the tested energy spectrum data, the mean values of the SNR and RMSE in Fig. 8 (a) and Fig. 8 (b) were 31.27 and 2.75, respectively, indicating that the denoising method used in this model was very effective.

The sample size also affects training accuracy. In this study, 500 standard spectra were selected as training samples, and preliminary model effect validation was performed. The PSO, SFLA, and stochastic gradient descent (SGD) are selected as controls. The convergence of the training process of each optimization model is shown in Fig. 9, where "Loss" represents the error of each iteration of the model, and "Epoch" represents the number of iterations of data in the training process.

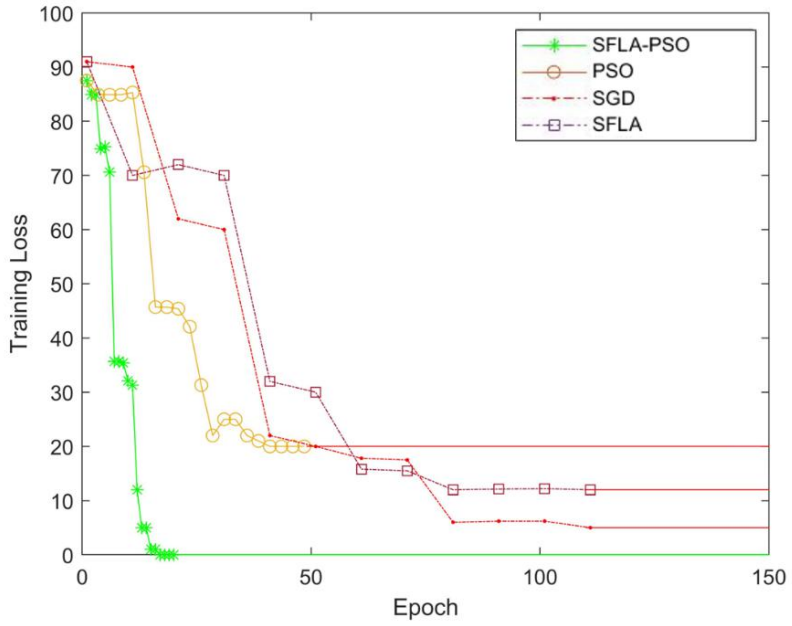

Fig. 9 Convergence of each optimization algorithm

It can be seen that the convergence of the four optimization models well reflects the characteristics of each model. Owing to the rapid convergence effect of the PSO algorithm, the neural network falls into local extrema, but the particle swarm optimization algorithm has completed convergence after 30 iterations; therefore, the prediction accuracy is low. The SFLA converges slower than the PSO, which converges to the local extrema approximately 75 times, but its accuracy is slightly higher than that of the PSO. When the CNN uses SGD to optimize the parameters, the convergence time is the longest, and approximately 110 iterations of convergence are completed. However, it is closest to the optimal extreme point, showing the possibility of falling into the local extreme value. The SFLA-PSO CNN model has the highest training efficiency, more than 20 iterations of convergence, and the best extreme value determination effect, which proves that this method has better nonlinear fitting ability and higher prediction accuracy for full-spectrum airborne gamma processing.

Increasing the dataset size is an important method of overfitting. Improve the accuracy of the model as much as possible and ensure its computational efficiency. In this study, 2000, 5000, and 10000 spectral data were used as samples for model training to obtain the most optimal model structure.

The sample training effect for each dataset size is shown in Fig. 10. With an increase in the sample size, the accuracy of the model also improved, and the training time was greatly improved. However, the models trained with different sample sizes converged when the loss tended to zero, indicating that the sample size had no significant influence on the accuracy of the model prediction ability. This is probably because this model only studies three types of nuclides, and there are few features to extract; therefore, ideal learning results can be obtained with a small number of samples. To obtain effective measurement efficiency and accuracy, an SFLA-PSO CNN model developed using 5000 samples was selected for this study.

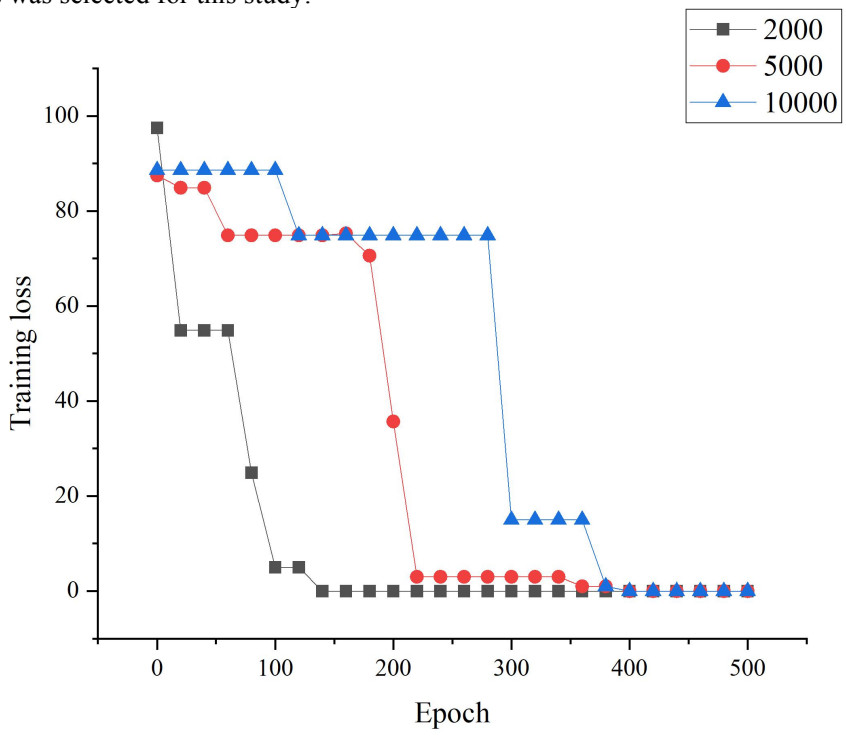

Fig. 10 Effects of training with different sample sizes

3.3 Application of measured spectrum in Saihangaobi mining area

After establishing the CNN, the network model was tested. The measured spectrum of the Saihangaobi Mining Area was used as the verification set to evaluate the model. The data file size was

87.7 M, the maximum count rate was 2636 cps, the minimum count rate was 2347 cps, and the average count rate was 2518 cps. The measurement files of the different lines contained at least 92 groups of spectral lines and at most 9243 groups. The average relative error was used as the evaluation method for the algorithm prediction effect, and the analysis results are shown in Fig. 11.

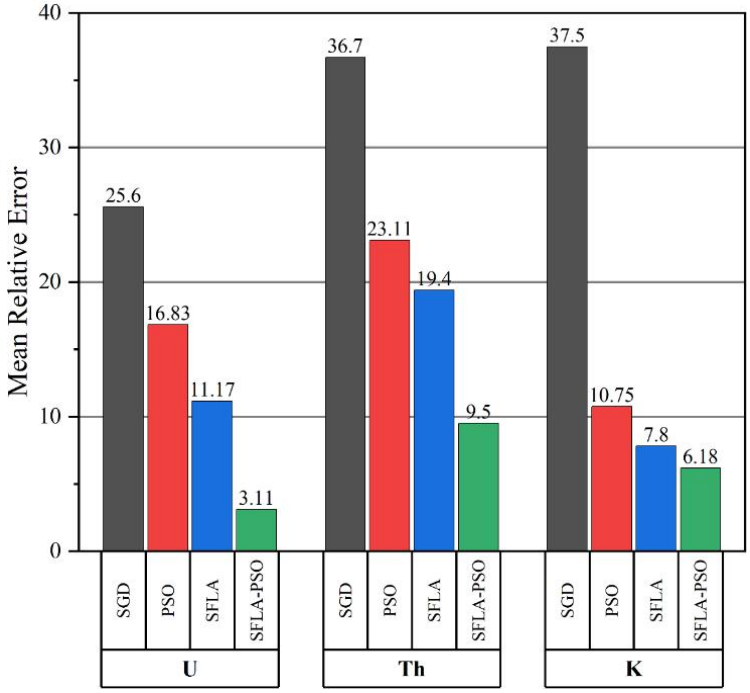

Fig. 11 Average relative error of peak area calculated by each optimization algorithm

The average relative errors of the peak areas of U, Th, and K obtained using the SGD method were 25.6%, 36.7%, and 37.5%, respectively; the relative error of the U peak was the smallest. Among the four optimizers, SGD exhibited the worst optimization ability, followed by the PSO method, with relative errors of 16.83%, 23.11%, and 10.75%, respectively, and its performance at the K peak was the best; then, the SFLA algorithm, with relative errors of 11.17%, 19.4%, and 7.8%, respectively, and its performance at the U peak was the best. Overall, SFLA-PSO had the best prediction effect on the U, Th, and K peak areas, which were 3.11%, 9.50%, and 6.18%, respectively, and are clearly better than those of the other three optimization algorithms. This result is related to the limitations of each algorithm. For the SFLA, the parameter determination is complicated and needs to be determined by several experiments; therefore, development of a reasonable scheme is necessary for design of the experiment, which has a significant impact on the actual effect of the SFLA. For PSO, similar to the SFLA, the coding of the network weight and selection of the genetic operator also significantly influence the results. For SGD, using only one sample for each iteration can guarantee training speed; however, it may yield a local minimum value with low accuracy.

To meet the actual demand for airborne radioactivity measurements, software programming was carried out in Python according to the algorithm model in this study, and data preprocessing was completed, including dead time correction, spectrum filtering, cosmic ray background calculation, and background deduction. The core part of the algorithm is used for the fitting calculation. To simplify the spectral data processing, a set of airborne gamma-ray spectral solution software was designed in this study. The operations include the following: “Import the.dat file,” display “Data to read,” and click “Output Folder” to select a path for saving calculation results. Click the “Calculate and save” button to save the results calculated by the mixed neural network in the “Results” folder under the selected path to complete the analysis process.

According to the Python logger running time, the single peak area calculation time is only between 0.13 and 0.15 ms in peak area batch processing, which fully meets the measurement

efficiency requirements under large sample conditions. Simultaneously, the calculated average relative errors of the peak areas of K, U, and Th were maintained at a fairly good level. According to the results in Fig. 3, the processing efficiency advantage of this algorithm is also relatively obvious. Thus, the proposed optimization algorithm was proven to be feasible in engineering practice, as evidenced by its performance in terms of convergence speed and prediction accuracy.

4. Conclusion

In this study, an SFLA-PSO CNN model for γ spectrum analysis was proposed. The model effectively employs the nonlinear mapping feature of the neural network to perform full analysis of the γ spectrum, and uses more spectral data to improve the analysis accuracy. This results in fairly high analysis efficiency and accuracy when the data signal is weak and the full-energy peak is not obvious, and the analysis of special spectrum lines can effectively denoise and highlight the weak peak information. Meanwhile, owing to the robustness of the neural network, data processing becomes simpler, some complex steps in data processing are omitted, and the time taken to calculate the peak area proves its fast processing capability. These advantages allow this method, particularly in the field of airborne gamma data processing, to quickly output nuclide content information, which is of great significance for aeronautical engineering surveying.

Acknowledgements

We thank the Sichuan Provincial Key Laboratory of Applied Nuclear Techniques in Geosciences and CDUT Team 203 for their English language review. We thank Professors Liang-quan Ge, David Cohen, Sheng-qing Xiong, and Si-chun Zhou for their support.

Data Availability Statement

Data will be made available on request.

Conflict of interest

The authors declare that they have no competing interests.

References

[1] International Atomic Energy Agency, *Airborne gamma ray spectrometer surveying (Technical Reports Series No. 323)* (International Atomic Energy Agency, Vienna (1991), from https://www.iaea.org/publications/1427/airborne-gamma-ray-spectrometer-surveying.

[2] Wan J.H., Xiong S.Q., & Fan Z.G. Technical status and prospect of airborne gamma spectrometry measurement. Geophysical and Geochemical Exploration (in Chinese), 2012, 36(03): 386-39. Retrieved in 2012, from https://www.wutanyuhuatan.com/CN/Y2012/V36/I3/386. DOI: 10.11720/wtyht.2012.3.12

[3] Xu Z.L., Meng Q.M., Li W.J., et al. Data processing Software System of airborne Geophysical Exploration Based on Oasis Montaj Platform. Computing Techniques for geophysical and geochemical Exploration (in Chinese), 2014, 36(03): 257-261. From https://d.wanfangdata.com.cn/periodical/wthtjsjs201403001. DOI: 10.3969/j.issn.1001-1749.2014.03.01

[4] Wang L.F., Xue D.J., He H., et al. Application of plug-in technology in GeoProbe geophysical software platform. Geophysical and Geochemical Exploration (in Chinese), 2013, 37(03): 547-551. From https://www.wutanyuhuatan.com/CN/Y2013/V37/I3/547. DOI: 10.11720/j.issn.1000-8918.2013.3.32.

[5] Wang P. & Dai L.J. (1992). Proceedings of the 8th Annual Conference of the Chinese Geophysical Society in 1992 (pp.170). Seismological Press. Retrieved on November 01, 1992.

[6] Guo Y.F., Ji A.G., Zhang Z.H., et al. Gamma energy spectrum processing technology research. Journal of daqing petroleum geology and development (in Chinese), 1993, 02: 56-60 + 8. Retrieved in 1993, from https://www.cnki.net/kcms/doi/10.19597/j.issn.1000-3754.1993.02.015.html. DOI: 10.19597/j.issn.1000-3754.1993.02.015

[7] Hendriks P.H., Limbur J., & Meijer R.J.D. Full-spectrum analysis of natural g-ray spectra. J. Environ. Radioactiv, 2001, 53(3): 365-380. Received on May 30, 1999, from https://doi.org/10.1016/S0265-931X(00)00142-9. DOI: 10.1016/S0265-931X(00)00142-9

[8] Guo Y.F. Smoothing and filtering of natural gamma spectrum. Journal of Daqing Petroleum Institute (in Chinese), 2003, 03: 113-114+117-128. Received on January 1, 2003, from http://xuebao.nepu.edu.cn/info/1242/6986.htm.

[9] Ni W.C. Theoretical study on the analysis method of airborne gamma-ray ful energy spectrum data. Uranium Geology (in Chinese), 2011, 27(04): 231-241.

[10] Gu Y, Sun K, Ge L.Q, et al.. Investigating the minimum detectable activity concentration and contributing factors in airborne gamma-ray spectrometry. Nucl. Sci. Tech. ,2021, 32(10): 30-38. Received on October 7, 2021, from https://link.springer.com/article/10.1007/s41365-021-00951-6 . DOI: 10.1007/s41365-021-00951-6.

[11] Jin Y, Guo Y, & Meng Y.X. Energy spectrum data processing and spectrum solving Method based on full spectrum. Electronic Technology and Software Engineering (in Chinese), 2018, 08: 164. From http://www.cqvip.com/QK/80675A/201808/675112991.html.

[12] Gu R.K, Hou Z.R, Shen E.S, et al.. Airborne monitoring of radioactivity level in the regions surrounding Qinshan nuclear power plant and Shanghai Radiation Protection. Radiation Protection (in Chinese), 1997, 17(3): 167-187. From http://www.cqvip.com/qk/91042x/19973/2512224.html.

[13] Pan Z.Q. Compilation of papers from the Fourth National Symposium on Nuclear Emergency Preparednes. Beijing: Papers from the fourth national symposium on nuclear emergency preparedness (in Chinese), 2006: 639-647.

[14] Ni W.C. & Gu R.K. Airborne monitoring method of nuclear emergency[J]. Uranium Geology (in Chinese), 2003, 19(6): 366-373. Received on November 10, 2003, from http://www.cqvip.com/QK/91728X/200306/8592358.html.

[15] Hou Z.R., Gu R.K., & Li J.J. Application of aerospace technology in nuclear accident emergency and environmental assessment. Proceedings of Baotou geophysical and geochemical Conference (in Chinese),1996, 1: 88-94.

[16] Ni W.C. Airborne selective gamma ray exploration. Uranium Gold Geology Abroad (in Chinese), 1997, 14(4): 344-351.

[17] Liu Q.S., Zhang Q.X., Yang H., et al.. Research on terrain correction method of airborne γ spectrometry. Nuclear Techniques (in Chinese), 2021, 44(9): 78-85. Received on May 20, 2021, from http://www.cqvip.com/QK/92722X/202109/7105563825.html. DOI: 10.11889/j.0253-3219.2021.hjs.44.090503.

[18] Xiong C., Sun K., Ge L.Q., et al.. A method for the identification of ore-caused anomalies information in the airborne γ-ray spectrum based on fractal filtering by layer. Nuclear Techniques (in Chinese), 2019, 42(1): 24-30. Received on September 26, 2018, from http://www.cqvip.com/QK/92722X/201901/7001139873.html. DOI: 10.11889/j.0253-3219.2019.hjs.42.010201.
[19] Ge L.Q., Zeng G.Q., Lai W.C., et al.. The development of a digital airborne gamma-ray spectrometry. Nuclear Techniques, 2011, 34(2): 156−160. Received in 2011, from https://www.hjs.sinap.ac.cn/thesisDetails?columnId=7184186&Fpath=home&index=0&lang=zh.
[20] Shao J.W., Bai L., & He L.X. Development of gamma spectrum processing software. Annual Report of China Institute of Atomic Energy (in Chinese), 2012, 00: 223.
[21] Lasche G., Coldwell R., & Metzger R. VRF ("Visual RobFit") -- nuclear spectral analysis with nonlinear full-spectrum nuclide shape fitting. EPJ Web of Conferences, 2017, 153: 1-6. Received on September 25, 2017, from https://doi.org/10.1051/epjconf/201715301002. DOI: 10.1051/epjconf/201715301002.
[22] Feng C.Y., Wang H.B., Zhou Z.Y., et al.. Application Research of airborne gamma full spectrum Analysis Method Based on Python Programming. World Nuclear Geology (in Chinese), 2022, 39(02): 280-288. Received in 2022, from http://www.cqvip.com/QK/96867A/202202/7107593147.html. DOI: 10.3969/j.issn.1672-0636.2022.02.011.
[23] Guo Y.F., Ji A.G., Zhang Z.H., et al.. Gamma energy spectrum processing technology research. Journal of daqing petroleum geology and development (in Chinese), 1993, 02: 56-60 + 8. Received in 1993, from http://www.cqvip.com/QK/91950X/199302/1004905.html. DOI: 10.19597/j.issn.1000-3754.1993.02.015.
[24] Zhou L.Y., Zha H., Shi J.R., et al.. A non-invasive diagnostic method of cavity detuning based on a convolutional neural network. Nucl. Sci. Tech. 2022, 33(7): 25-35. Received on April 07, 2022, from https://doi.org/10.1007/s41365-022-01069-z. DOI：10.1007/S41365-022-01069-Z
[25] Jin J.Q., Yu C.C., Shi L., et al.. Review on integration technology of foreign airborne geophysical exploration systems (2015-2020). Geophysical and Geochemical Exploration (in Chinese), 2022, 46(02): 285-295. From http://www.cqvip.com/QK/95670X/202202/7106928664.html.
[26] Yao Y.J. Based on a large sample of gamma ray bursts delay spectrum research. Master dissertation. Shijiazhuang: Hebei normal university, Shijiazhuang, 2021.
[27] Gao H.B., Gao L., Zhou C., et al.. Research on Neural Network Training Algorithm based on Particle Swarm Optimization. Acta Electronica Sinica (in Chinese), 2004, 32(09): 1572-1574. From http://www.cqvip.com/QK/90131X/200409/10411371.html.
[28] Yang T., Zhou H.Y., & Guan L.T. Adaptive wavelet Threshold denoising method for vibration Suppression. Journal of Chinese Universities (Natural Science) (in Chinese) , 2005, 44(06): 15-19.
[29] Zhang L., Qin H.F., & Yu C.B. Research on Denoising Algorithm based on Wavelet Threshold. Computer Engineering and Applications (in Chinese), 2008, 09: 172-173+199. From http://www.cqvip.com/QK/94631X/200506/20788935.html.
[30] Donoho D.L., & Johnstone I.M. Ideal Spatial Adaptation by Wavelet Shrinkage. Biometrika, 1994, 81(3): 425-455. From https://doi.org/10.1093/biomet/81.3.425. DOI: 10.1093/biomet/81.3.425
[31] Sun K., Xiong C., Ge L.Q., et al.. Method of line element correction for airborne γ spectrum anomaly information based on wavelet transform. Nucl. Technol. 2018, 41(10): 43-49. Received on June 20, 2018, from https://www.hjs.sinap.ac.cn/thesisDetails#10.11889/j.0253-3219.2018.hjs.41.100501&lang=zh. DOI: 10.11889/j.0253-3219.2018.hjs.41.100501.
[32] Lin T., Mi Y.H., Yang M.P., et al.. Research on Airborne Gamma Spectrum Data Denoising Method Based on VMD-Wavelet Threshold. Geological Review (in Chinese), 2021, 67(S1): 199-200. From http://www.cqvip.com/QK/91067X/2021S01/00002H8CL15O7JP0MN508JPVM7R.html. DOI: 10.16509/j.georeview.2021.s1.088.
[33] Li F., Guo W.T., Deng X.T., et al.. A Hybrid Shuffled Frog Leaping Algorithm and Its Performance Assessment in Multi-Dimensional Symmetric Function. Symmetry, 2022, 14(1): 131. Received on December 08, 2021, from https://doi.org/10.3390/sym14010131. DOI: 10.3390/sym14010131.
[34] Mohamed S.E.T. Advanced algorithms for retrieving pileup peaks of digital alpha spectroscopy using antlions and particle swarm optimizations. Nucl. Sci. Tech. 2020, 31(4): 47-68. Received on November 06, 2019, from https://doi.org/10.1007/s41365-020-0745-5. DOI: 10.1007/s41365-020-0745-5.
[35] Li S., Liu L.J., & Zhai M. Short-term Traffic Flow Prediction Based on BP Neural Network based on Improved Particle Swarm Optimization. Systems Engineering Theory & Practice (in Chinese), 2012, 32(09):

2045-2049. From http://www.cqvip.com/QK/95538X/201209/43275980.html. DOI: 10.12011/1000-6788(2012)9-2045.
[36] Long Q., Liu Y.Q., & Yang Y.P. Wind Turbine Gearbox Fault Diagnosis Method Based on Particle Swarm Optimization BP Neural Network. Journal of Solar Energy (in Chinese), 2012, 33(01): 120-125. From http://www.cqvip.com/QK/95586X/201201/40734445.html.
[37] Zhou W.H. Research on Hidden Layer Structure and Parameter Optimization of RBF Neural Network. Master dissertation. Shang Hai: East China University of Science and Technology, 2014.
[38] Zhang Y.J., Jin P.J., Fu X.H., Zhang F.C., Hou J.R., & Xu J.R.. Feature Extraction of Multi-peak Brillouin Scattering Spectrum Based on SFLA-LSSVM Algorithm[J]. Chinese Journal of Lasers (in Chinese), 2018, 45(1): 0106004. From https://www.opticsjournal.net/Articles/OJf66ebd3bab511abd/Abstract. DOI: 10.3788/CJL201845.0106004.
[39] Ge L.Q., Xiong S.Q., Zeng G.Q., et al. The reading environment: Airborne Gamma Spectrum Detection Technology and Application. Gloucestershire: Science Press (in Chinese), 2016. Retrieved in August, 2016, from https://book.sciencereading.cn/shop/book/Booksimple/show.do?id=B1BFE49D395CB4C6F90E9408E8C6033F6000.
[40] Pang J.F. The reading environment: γ Spectrum data analysis. Gloucestershire: Shaanxi Science and Technology Press (in Chinese), 1990). Retrieved in 1990.
[41] Kayalvili S., & Selvam M. Hybrid SFLA-GA algorithm for an optimal resource allocation in cloud. Cluster Computing, 2019, 22(2): 3165. Received on December 25, 2017, from https://doi.org/10.1007/s10586-018-2011-8. DOI: 10.1007/s10586-018-2011-8.
[42] Minty B.R.S. Airborne gamma-ray spectrometric background estimation using full spectrum analysis. Geophysics, 1992, 57(2): 279-287. Received on February 21, 1991, from https://doi.org/10.1190/1.1443241.
[43] Li F., Tang C.F., Li H., et al.. A LLS operator based S-I WT de-noising algorithm applied in EDXRF. X-ray Spectrom, 2023, 52(1): 13-21. From https://doi.org/10.1002/xrs.3159. DOI: 10.1002/xrs.3159.